Geophysical Research Letters

Key Points:
- Precise locations of 390,334 aftershocks of the 2016–2017 Central Italy sequence illuminate the complex normal fault system
- A system of high-angle bookshelf faults accommodates slip at the intersection between normal and detachment faults
- A deep-reaching seismic barrier is identified north of the Sibillini Thrust that may control the ruptures of large earthquakes

Fault Planes, Fault Zone Structure and Detachment Fragmentation Resolved With High-Precision Aftershock Locations of the 2016–2017 Central Italy Sequence

Felix Waldhauser[1] , **Maddalena Michele[2]** , **Lauro Chiaraluce[2]** , **Raffele Di Stefano[2]**, and **David P. Schaff[1]**

[1]Lamont-Doherty Earth Observatory of Columbia University, Palisadesm, NY, USA, [2]Istituto Nazionale di Geofisica e Vulcanologia, Rome, Italy

Abstract Three devastating earthquakes of $M_W \geq 5.9$ activated a complex system of high-angle normal, antithetic, and sub-horizontal detachment faults during the 2016–2017 central Italy seismic sequence. Waveform cross-correlation based double-difference location of nearly 400,000 aftershocks illuminate complex, fine-scale structures of interacting fault zones. The Mt. Vettore–Mt. Bove (VB) normal fault exhibits wide and complex damage zones, including a system of bookshelf faults that intersects the detachment zone. In the Laga domain, a comparatively narrow, shallow dipping segment of the deep Mt. Gorzano fault progressively ruptures through the detachment zone in four subsequent $M_W \sim 5.4$ events. Reconstructed fault planes show that the detachment zone is fragmented in four sub-horizontal, partly overlaying shear planes that correlated with the extent of the mainshock ruptures. We find a new, deep reaching seismic barrier that coincides with a bend in the VB fault and may play a role in controlling rupture evolution.

Plain Language Summary In 2016–2017, a sequence of three devastating earthquakes with magnitudes ~6 near the towns of Amatrice, Visso, and Norcia in central Italy triggered hundreds of thousands of aftershocks. We compute high-precision locations for these aftershocks that have the power to illuminate the fine-scale structure of the complex system of intersecting and interacting faults that were activate during the sequence. The normal faults that ruptured during the three mainshocks are capped at ~9 km depth by a sub-horizontal detachment zone. The normal faults intersect the detachment at an acute angle, causing complex fault zone structures and fragmentation of the detachment where they intersect. We observe a deep reaching seismic barrier that we conclude may play a role in controlling rupture extent and evolution of large earthquakes along this section of the Apennines. In general, fault complexity here is higher than in similar sequences in 2009 near L'Aquila to the south and in 1997 near Colfiorito to the north.

1. Introduction

The 2016–2017 earthquake sequence in central Italy has been one of the most vigorous and best recorded seismic events along the Apennine mountain chain. As frequently observed in regions of distributed continental faulting (Walters et al., 2018), the sequence was characterized by a series of large normal faulting earthquakes that span over a period of only a few months. The complex nature of the cascade of multi-segment fault ruptures resembles previous large (e.g., 1980, Irpinia, 1997 Colfiorito, 2009 L'Aquila; see Chiaraluce et al., 2017 and references therein) and smaller sequences (e.g., Sánchez-Reyes et al., 2021; Totaro et al., 2015) along the Apennines, all related to a network of interconnected and highly segmented active normal faults that respond to the present-day extensional stress field and interact with thrust structures inherited from a compressional tectonic phase during the Neogene.

The 2016–2017 sequence ruptured the 80 km long normal fault system in three mainshocks between August and October 2016, activating segments of the Mt. Vettore-Mt. Bove Fault system (VBFS) north of the Sibillini Thrust (ST), and of the Mt. della Laga Fault system (LFS) south of the ST (Figure 1a). It started with a M_W6.0 on August 24, 2016 (01:36 UTC) that nucleated near the town of Amatrice at the northern end of the LFS, presumably on the Mt. Gorzano fault. Most of the slip (and all surface rupture, Villani et al., 2018) occurred on the VBFS, however. The Amatrice event is followed by a M_W5.9 on October 26, 2016 (19:18
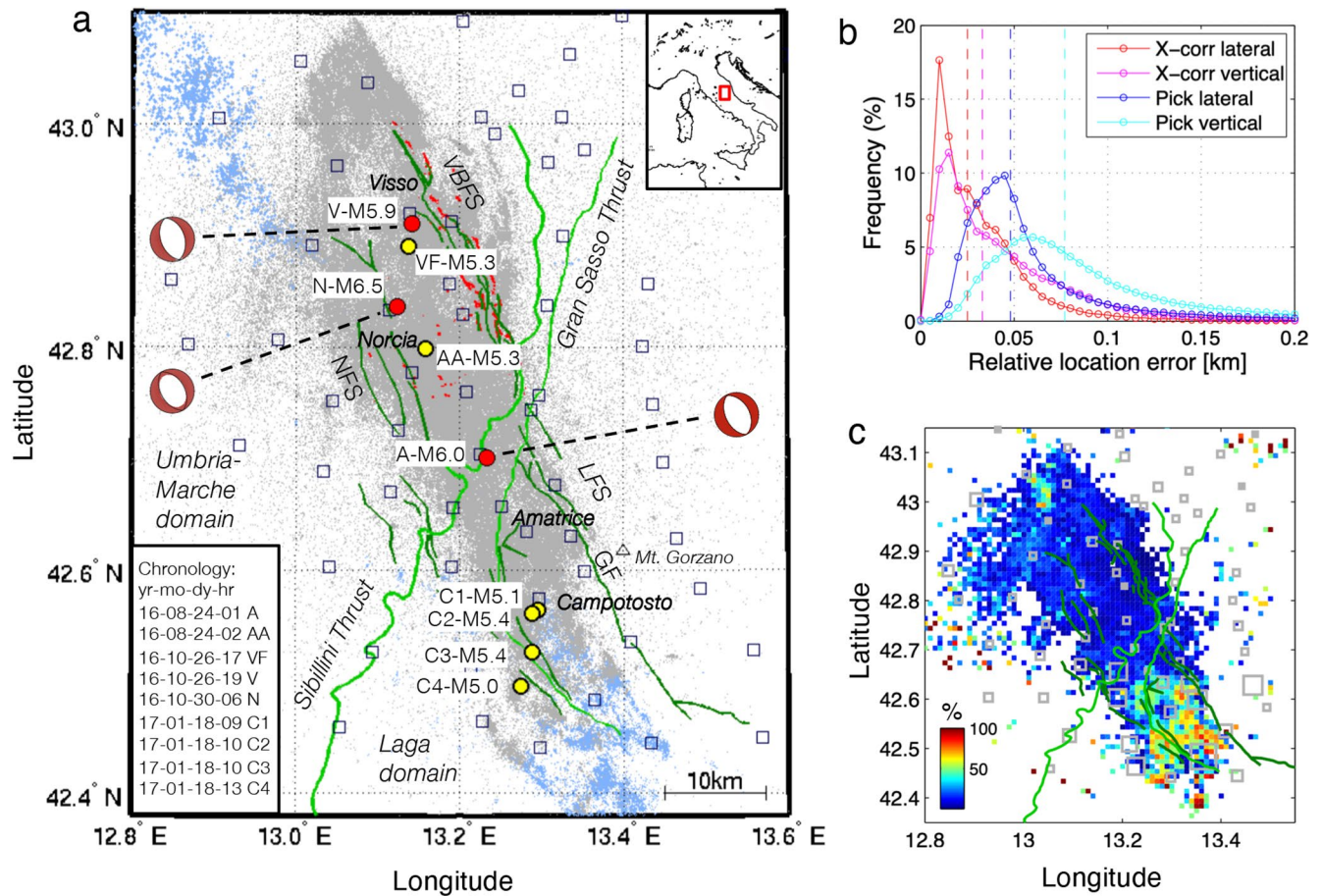
Figure 1. (a) Map of seismic stations used in this study (squares) and 390,334 epicenters after relocation (gray dots). Red dots denote the location of the Amatrice , Visso, and Norcia mainshocks, yellow dots locations of the Amatrice aftershock, the Visso foreshock; and the four Campotosto events (C1-C4). Light blue dots are aftershocks of the 1997 Colfiorito and 2007 L'Aquila earthquakes. Focal mechanisms for the three mainshocks are from Scognamiglio et al. (2009). Dark green lines are mapped normal faults, light green thrust faults (Pucci et al., 2017). Red lines are mapped surface ruptures (Villani et al., 2018). VBFS: Mt. Vettore–Mt. Bove Fault System; NFS: Norcia Fault System; LFS: Laga Fault System; GF: Mt. Gorzano Fault. Inset in upper right corner shows study area (red box), in lower left corner date and time of occurrence of events shown as red and yellow dots. (b) Distribution of relative location errors (i.e., the horizontal and vertical projections of the 95% confidence ellipses) from a bootstrap analysis of 200 samples of the final delay time residual for events constrained mainly by pick and those mainly constrained by correlation data. Dashed lines indicate median values. (c) Percentage of correlated events (pairs with at least three seismograms with correlation coefficients ≥0.7) within bins of 1 × 1 km. Open squares show stations with correlation measurements, scaled by number of measurements (largest square: ~200,000 measurements), small solid squares stations without correlation data.

UTC) that ruptured the VBFS near Visso in the north. Four days later, on October 30, 2016 (06:40 UTC), the largest event with $M_w6.5$ nucleated on the Mt. Vettore fault between the two previous events near the town of Norcia. It ruptured the entire length of fault area between Amatrice and Visso, including portions of the fault that slipped in the previous events and possibly the NNE trending section of the ST (Scognamiglio et al., 2018). The sequence culminated on January 18, 2020 in a series of four events with $5.0 \leq M_W \leq 5.5$ (C1-C4 in Figure 1a) that ruptured the southernmost portion of the fault system near Campotosto at the northern termination of the 2009 L'Aquila rupture. Other notable events include a M_W 5.3 aftershock (AA in Figure 1a) that occurred 1 h after the Amatrice event on an antithetic fault (Chiaraluce et al., 2017), and an $M_W5.4$ foreshock (VF in Figure 1a) that preceded the Visso mainshock by 2 h.

In a joint effort between Italian and UK government institutions and universities, a rapidly expanding network of more than 130 permanent and temporary stations was deployed soon after the Amatrice mainshock (Moretti et al., 2016; Figure 1a). Initial hypocenter parameters were routinely computed in near-real time by the Istituto Nazionale di Geofisica e Vulcanologia (INGV) (ISIDe Working Group, 2007), followed by subsequent catalog improvements with respect to completeness and/or location resolution (Chiaraluce

et al., 2017; Improta et al., 2019; Michele et al., 2016, 2020; Spallarossa et al., 2020; Tan et al., 2021). The general picture revealed by this and other studies is that of a complex fault system, composed of two main, sub-parallel, NNW striking and west-dipping, segmented normal faults (VBFS and LFS). The normal fault system is transected by the inherited, NNE striking ST (Cooper & Burbi, 1986; Koopman, 1983; Lavecchia, 1985; Mazzoli et al., 2005; Porreca et al., 2020) and the Gran Sasso Thrust (e.g., Ghisetti & Vezzani, 1991), along which both the Umbria-Marche Carbonatic domain, which represents the northern lithological succession, and the Gran Sasso domain in the south-east, overthrust the Laga domain, which mainly consists of turbidites (Centamore & Rossi, 2009) (Figure 1a). In the depth range of 8–10 km the normal faults are truncated by a sub-horizontal, slightly east-dipping band of seismicity (Chiaraluce et al., 2017) interpreted as a detachment shear zone (Vuan et al., 2017).

Here we relocate the Spallarossa et al. (2020) catalog to develop a cross-correlation based double-difference catalog of nearly 400,000 aftershocks with unprecedented location precision down to a minimum magnitude of completeness (Mc) of 0.6. We focus our analysis on fine-scale fault structural details that help improve our understanding of the nature of the detachment shear zone and its complex interaction with the intersecting normal faults. We harness the increased spatio-temporal resolution of the sequence to investigate the presence of seismic barriers that control aftershock propagation and possibly rupture evolution.

2. Data and Analysis

Our initial data set comprises the catalog of 447,482 earthquakes of Spallarossa et al. (2020) from August 24, 2016 (the date of the Amatrice mainshock) and August 31, 2017, when the UK temporary stations were removed (Moretti et al., 2016). The catalog is based on 17 million P- and S-wave picks, derived from applying an automatic picker to the continuous waveform data. A grid search method (NonLinLoc; Lomax et al., 2000) together with station corrections and depth-dependent P- and S-velocity models (De Luca et al., 2009) were used to estimate absolute locations (see Spallarossa et al., 2020 for details). The catalog includes magnitudes that range from M_L −1.0 to M_W 6.5, with a minimum magnitude of completeness, Mc = 0.6.

We relocate the Spallarossa et al. (2020) catalog by using the double-difference code HypoDD (Waldhauser, 2001) to invert, in an iterative, weighted least squares sense, phase delay time residuals observed at common stations for precise relative distances between the hypocenters (Waldhauser & Ellsworth, 2000). To ensure location robustness and preserve catalog completeness we select all those events that have at least four P-wave arrival time picks and at least six picks in total. In addition to delay times formed from picks of events with hypocenters separated by less than 8 km, we compute 92 million high-precision delay times for all event pairs separated by less than 2 km by cross-correlating pairs of filtered (1–15 Hz) seismograms with correlation coefficients $Cf \geq 0.7$ using 0.5 and 0.7 s long P- and S-wave windows, respectively (see Schaff & Waldhauser, 2005 for details). As the precision of correlation delay times decreases with decreasing Cf (Figure S1a), measurements from seismograms with Cf below our chosen threshold of 0.7 are generally less precise than the corresponding pick delay times and prone to cycle skipping and the correlation of noise (see Michele et al., 2020; Waldhauser & Schaff, 2008). We predict the delay time data with the 1-D P- and S-velocity-depth functions used by Michele et al. (2020) (Figure S1b), which are a finely layered representations of the gradient models derived by Carannante et al. (2013).

The high-rate and high-density catalog is relocated using a length-scale dependent, spatial and random sub-sampling approach. We form regions of approximately 10 × 10 km that overlap by 80% and relocate each region individually (see Waldhauser & Schaff, 2008). In regions with more than 10,000 events we randomly subsample the events to form batches of 10,000 events and relocate each batch. We repeat that process 10 times to ensure a uniform delay time linkage between events (see Waldhauser et al., 2020 for details). Finally, we merge all relocated hypocenters by taking the mean in multiple locations of the same event, linearly weighted by the normalized distance from their centroid, to compute a final catalog of 390,334 relocated earthquakes.

Relative location uncertainties are derived from a bootstrap analysis of 200 random samples taken from the final double-difference residual vector in each box (see Waldhauser & Ellsworth, 2000, for details). Median horizontal and vertical errors are 0.048 and 0.077 km, respectively for events mainly constrained by
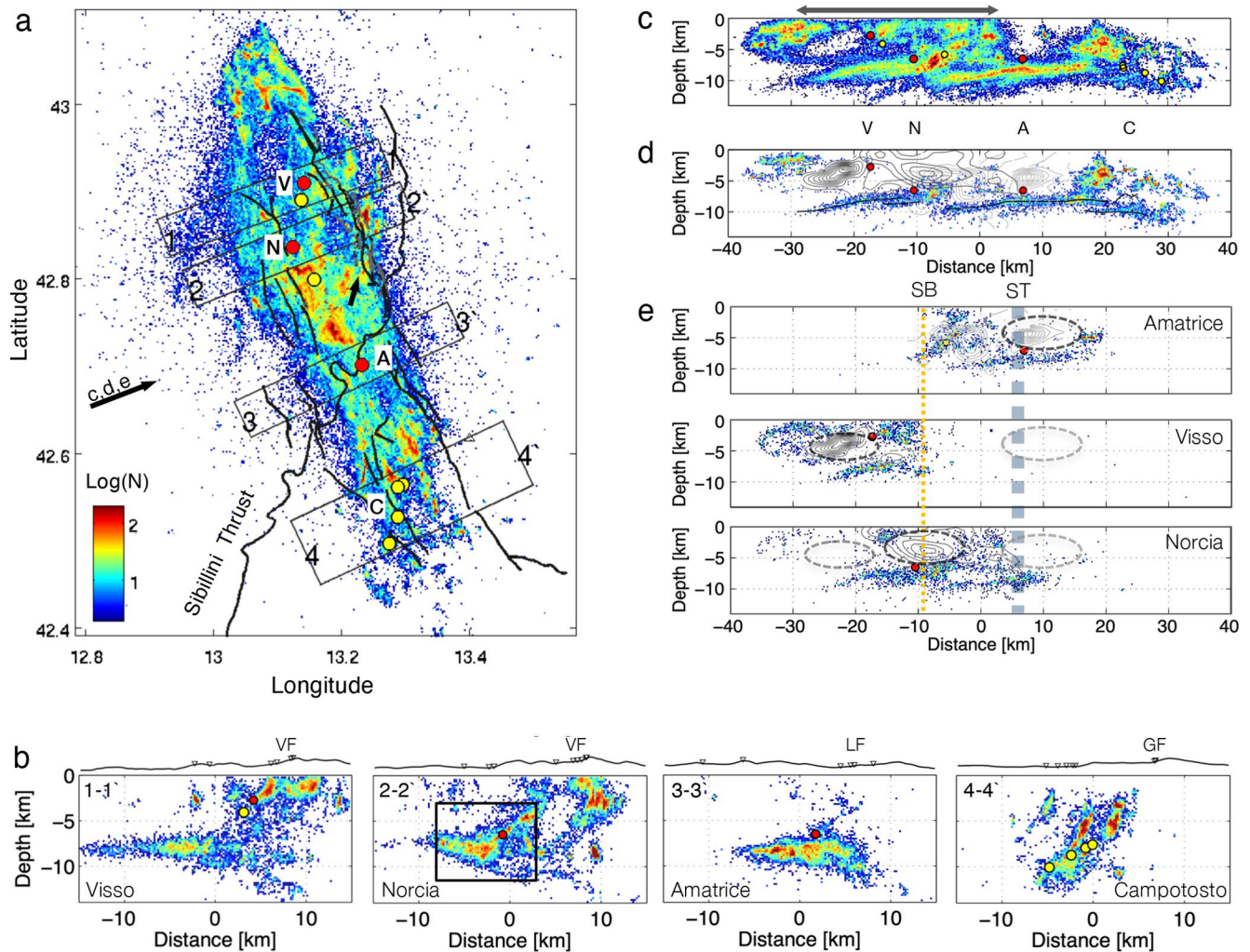
Figure 2. Density of relocated earthquakes shown in (a) map view, (b) fault perpendicular cross sections, and (c,d,e) fault longitudinal cross sections looking ENE. Densities are shown as the log number of events within 0.2 × 0.2 km cells. Only cells with more than three events are shown, and the maximum number of events in a cell is capped at 200 to enhance structure (the largest cell has 457 events). In (a) black lines are mapped faults (Villani et al., 2018) and annotated rectangles include events shown in cross sections in (b). Labeled arrow shows projection direction for events shown in (c)–(e). Arrow near center of figure points to bend in Mt. Vettore–Mt. Bove fault (see text). In (b) triangles denote surface trace location on top of topographic relief. Box in cross section 2-2` shows area shown in Figure 4a. In (c) all events are included, in (d) only pairs of events that correlated with at least 10 cross-correlation measurements at a coefficient threshold ≥0.7. Red dots are mainshocks near Amatrice, Visso, Norcia, and yellow dots Amatrice aftershock, Visso foreshock, and events near Campotosto. In (e) 4 days of aftershocks are shown for each of the three mainshocks. Gray dashed line is projected location of Sibillini Thrust, yellow dashed line location of proposed seismic barrier (SB), dashed ellipses approximate areas that ruptured during the three mainshocks. Gray lines in (d) and (e) are slip contours for the three mainshocks (from Chiaraluce et al., 2017; Tinti et al., 2016).

arrival time picks (Figure 1b). Median errors for events mainly constrained by correlation data are 0.025 km in horizontal and 0.033 km in vertical direction. These values are similar to an analysis of the scatter in the multiple locations for each event in the overlap regions, which have medians (means) of 0.053 km (0.076 km) in horizontal and 0.075 km (0.121 km) in vertical directions.

3. Results

3.1. Hypocenter Locations

Because of the high density of hypocenters, the location of faults that host most of the seismic activity is best viewed by plotting the density of events instead of the individual hypocenters (Figure 2 and Figure S2). Consistent with previous studies (Chiarabba et al., 2018; Chiaraluce et al., 2017; Improta et al., 2019; Michele

et al., 2020; Tan et al., 2021), the new catalog images a series of complex, segmented WSW dipping normal faults within the VBFS and LFS (Figures 2a and 2b) that also involve slip on antithetic faults (Figure S2b, Sections 2, 6, 8-10; see also Michele et al., 2020), and brittle movement within a sub-horizontal shear zone that terminates the normal faults at 8–10 km depths and extends over much of the study region (Figure 2c). The active fault surfaces also include areas that are devoid of seismicity mainly related to the main slipping patches (Figures 2a, 2c and 2e; Chiaraluce et al., 2017; Tinti et al., 2016) in agreement with the anti-correlation of slip and aftershocks seen elsewhere (e.g., Mendoza & Hartzell, 1988).

3.2. Correlated Events

Earthquakes that slip in the same or nearby fault patches with similar rupture characteristics ought to generate similar waveforms at common stations, assuming a time-invariant velocity structure between sources and observing station. An abundance of such correlated earthquakes typically indicates smooth faults that slip repeatedly, while a scarcity of correlated events, especially in areas with high event density, points to inherent complexity of seismogenic structures (e.g., Waldhauser & Schaff, 2008). Here, we define correlated events as events that share at least two seismograms with $Cf \geq 0.7$ with each of at least five neighboring events. Our results do not change significantly when choosing higher Cf thresholds or more correlated neighboring events.

Correlated events exist predominantly south of the ST in the Laga Domain (Figure 1c), on normal fault segments activated during both the January 18, 2017 series of $\sim M_W 5$ Campotosto events and the 2016 Amatrice M_W 6.0, and also during the 2009 L'Aquila M_W 6.1 seismic sequence. The lack of correlated aftershocks along normal faults north of the ST (Figures 1c and 2d) indicates strong source and/or structural heterogeneities over short spatial scales. This is consistent with the complex mainshock ruptures (e.g., Scognamiglio et al., 2018) and tectonic processes in the Umbria-Marche Domain. Earthquakes south of the ST generate correlated waveforms at stations south of the ST, but to a much lesser extent north of it (see squares in Figure 1c). This suggests that the thrust structure acts as a scatterer for seismic waves passing through it.

Correlated events are abundant within sub-horizontal bands of seismicity in the 7–11 km depth range (Figure 2d). There they concentrate along narrow (100s of meters) faults within the more broadly active, fragmented detachment zone. These shear faults can be traced between 42.5–43°N and partially overlay in the Campotosto region (20 km model distance, Figure 2d) and beneath the Norcia hypocenter (−10 km model distance). The detachment structure is characteristic for this part of the Apennine fault system and cannot be detected as seismically active structure north (Chiaraluce et al., 2003; 1997 Colfiorito) and south (L'Aquila 2009: Chiaraluce, 2012) of the study region.

3.3. Fault Planes and Detachment Surfaces

We reconstruct the normal fault planes by applying a principle component analysis (PCA) to 2 months of aftershock locations within approximately 6 km from the hypocenters of the Amatrice, Visso, and Norcia mainshocks, the M_W 5.3 Amatrice aftershock, and the M_W 5.4 earthquake of 2017/01/18 (UTC 10:25:24) on the Campotosto fault (Figure 3a). The PCA planes' strike and dip are consistent with those from available moment tensor solutions for the main events (Scognamiglio et al., 2009). The surfaces of the sub-horizontal detachment fault segments were reconstructed by averaging the depths within the narrow bands of correlated events shown in Figure 2d that define repeated slip on the detachment interface. Average depths are computed within lateral bins of 1×1 km and then interpolated and shown as sub-horizontal surfaces in Figure 3a.

Using the reconstructed fault planes, we measure the width of the damage zone surrounding the core (i.e., the main slipping plane) of the normal faults by computing the orthogonal distances of aftershocks from the fault surfaces, choosing aftershocks of $M_L \geq 0.6$ ($\sim M_C$) that occurred within 1.5 km from either side of the fault plane and within 10 days of each of the three mainshocks, the Amatrice aftershock, and the M_W 5.4 Campotosto event (Figure S3). Following Valoroso et al. (2014) we define damage zone widths as $2 \times$ the standard deviation of each distribution, yielding values between 0.91 and 1.74 km. The scaled bar heights in the histograms are fit with a Weibull distribution using maximum likelihood to account for the asymmetry in the distribution (Figure S2). The Weibull curves show a tendency to wider damage zones
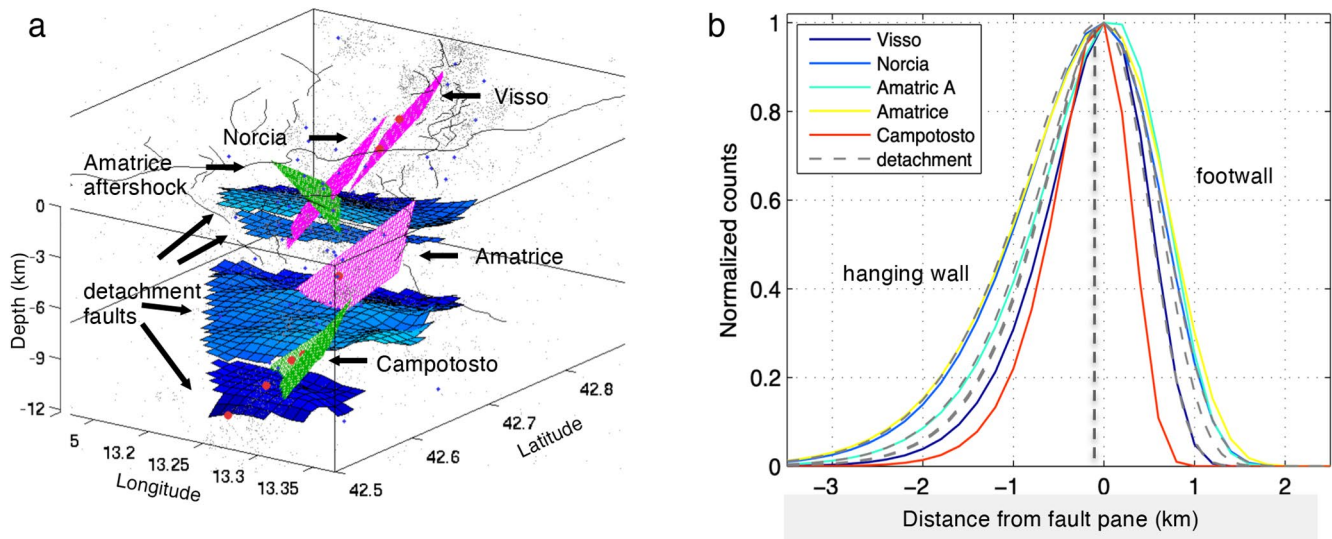
Figure 3. (a) 3D perspective view of principle component analysis (PCA) derived normal fault planes for the three mainshocks near Amatrice, Visso, and Norcia (magenta), the Amatrice foreshock and the M_W 5.4 earthquake of 2017/01/18 (UTC 10:25:24) on the Campotosto fault (green). Surfaces of the sub-horizontal detachment faults (blue) are computed from the location of correlated events (Figure 2d). Gray lines at surface are mapped fault traces. (b) Normalized distribution of fault orthogonal distances (100 m bins) of aftershocks from each of the PCA derived fault planes and detachment fault surfaces shown in (a). Negative distances are events in hanging wall and above sub-horizontal detachment surface, positive in footwall and below detachment surface.

toward the center of the fault system which ruptured in the Amatrice and Norcia events (Figure 3b). They further show an asymmetric distribution, consistent with previous studies on normal faults that observe wider damage zones in the hanging wall compared to the footwall (e.g., Berg & Skar, 2005). Estimates for the detachment faults are computed in the same way, yielding 2 × standard deviations between 1.17 and 1.47 km (Figure 3b).

4. Discussion and Conclusion

4.1. Seismic Barrier

The 2016–2017 central Italy sequence reflects the multiphase evolution of the Apennine orogen, in which the compressional regime active during the Neogene is overprinted by extensional tectonics that started in the Early Pleistocene (Barchi et al., 2012; Buttinelli et al., 2021; Calamita et al., 2012; Cavinato & De Celles, 1999; Cosentino et al., 2017; Lavecchia et al., 1994, 2002). From a regional-tectonics perspective the 2016–2017 sequence appears to be an overdue failure of a section of the Apennine fault system that has ruptured to the north near Colfiorito in 1997 (Chiaraluce et al., 2003) and to the south near L'Aquila in 2007 (Valoroso et al., 2013) (Figure 1a). It is unclear why it did not fail in a single event, although fault complexity and Coulomb stress transfer have been shown to play a role in the sequence's evolution (Mildon et al., 2017; Pino et al., 2019).

The ST has been proposed to control rupture initiation and arrest of the mainshocks (Barchi et al., 2021; Improta et al., 2019; Tinti et al., 2016), although the Amatrice rupture crossed it. Chiaraluce et al. (2017) proposed that rheological heterogeneities within the source volume controls slip distribution. Specifically, the same tectonic history may still result in local heterogeneous pre-stress distribution resulting in different yield and frictional stress along specific fault portions, generating an interplay between asperities and barriers (Page et al., 2005). Longitudinal cross-sections showing 4 days of aftershocks following the three mainshocks (Figure 2e) reveal a sharp seismic barrier (SB, yellow dashed line in Figure 2e), about 15 km north of the Sibillini Thrust, that marks the northern and southern termination of Amatrice and Visso aftershocks, respectively. Surprisingly, the barrier stops aftershocks on both normal and detachment faults, suggesting a deep reaching feature. A Coulomb stress analysis (Mildon et al., 2017) indicates that a nearby bend in the Mt. Vettore fault (arrow in Figure 2a) appears to act as a stress barrier. The Norcia earthquake nucleated
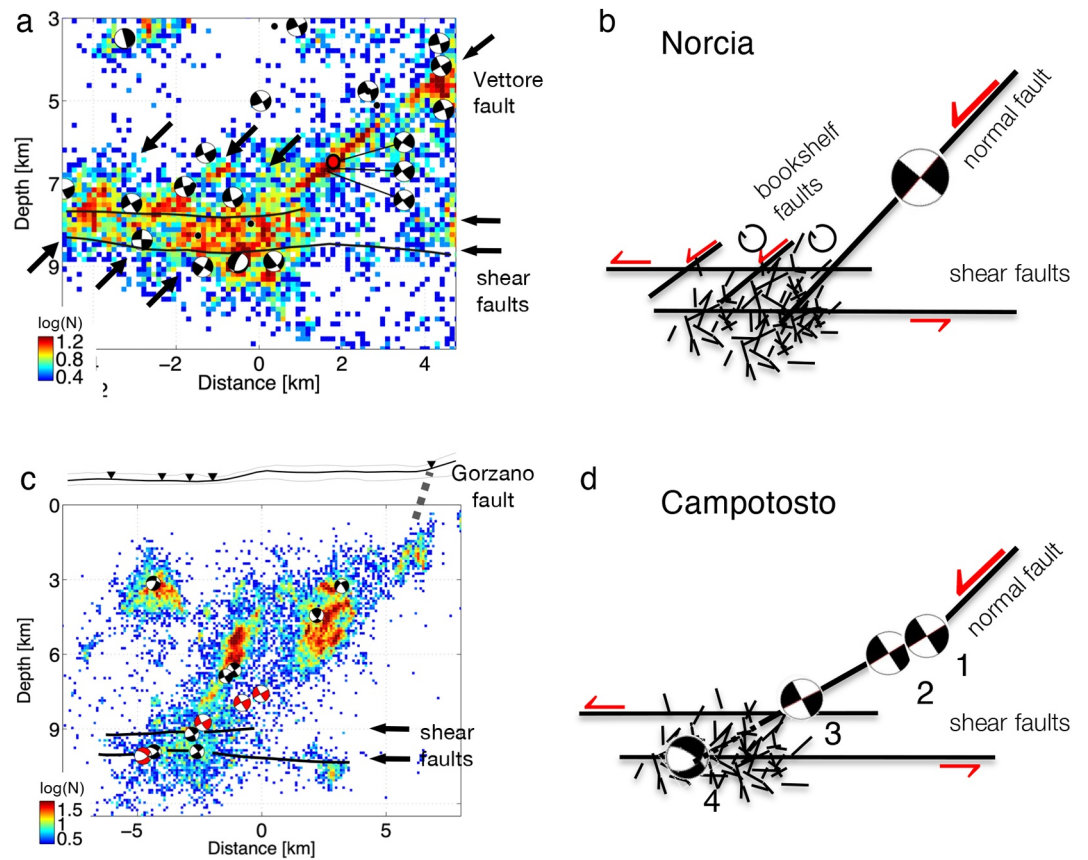
Figure 4. Event density plots (a), (c) and fault model sketches (b), (d) focusing on the intersection between normal and detachment faults at the base of the Mt. Vettore fault (a) and the Campotosto fault (c). Black lines in (a) and (c) are the location of the detachment faults derived from correlated events (see text and Figure 2d), arrows point to faults discussed in text. Numbers in (d) indicate timing of occurrence (see lower-left inset of Figure 1a). Focal mechanisms from waveform (Scognamiglio et al., 2009) and moment tensor inversion (Malagnini & Munafò, 2018) in (a), (c) are side projections onto cross sections.

close to the barrier and ruptured to either side of it in a high slip and stress-drop event (Supino et al., 2019). Most of its aftershocks reactivated the structures that were active in the Amatrice and Visso events.

4.2. Intersecting High-Angle Normal and Detachment Faults

An unresolved question in understanding the fault system is the interaction between the high angle normal faults that slip in major earthquakes and the detachment faults that slip in small earthquakes. Vuan et al. (2017) showed that most of the seismic activity in the months leading up to the sequence's onset occurred along the detachment fault, with increasing activity on the detachment fault preceding slip on the normal faults. The authors interpreted this pattern as the brittle signature of tectonic loading of the detachment and subsequent unlocking portions of the overlaying higher angle normal faults. During the sequence, on the other hand, we observe earthquakes along the detachment to occur in response to movement on the normal faults. In Figure 2e (and further described below) this can be seen in the activation of the detachment right below and in the days after each mainshock. Thus, while movement on the detachment fault may have started the sequence, the detachment responded passively to slip on the normal faults during the sequence.

Figure 4a shows a close-up image of seismicity at the base of the Mt. Vettore fault that ruptured in the Norcia event, where it intersects the two sub-horizontal faults that are separated in depth by about 800 m and make up the detachment zone at this location (see Figure 2d). Strong, diffuse seismic activity and diverse focal mechanisms (Malagnini & Munafò, 2018; Scognamiglio et al., 2009) within and just below

the detachment zone indicate that the Mt. Vettore fault penetrates the shear zone, causing a ~1 km thick band of complex faulting. Several shorter, progressively shallower dipping normal faults (see black arrows in Figure 4a) intersect the detachment faults west-southwest of the Mt. Vettore fault. These normal faults are about 1 km apart and suggest that they bound uniformly tilted blocks that resemble bookshelf-type systems with horizontal rotation axes characteristic of extensional regimes (Figure 4b) (e.g., Wernicke & Burchfield, 1982). Similar structures have been activated during the 2010–2013 Pollino earthquake swarm in the southern Apennines and interpreted as an extensional duplex that may have reactivated a pre-existing compressional structure (Totaro et al., 2015).

In the southernmost portion of our study region, a depth section across the Laga fault system shows that the seismicity is compatible with the geometry of the Mt. Gorzano fault. Previously unresolved, the new catalog unambiguously shows that the Mt. Gorzano fault is active and continuous throughout the whole entire crust (Figure 4c), progressively dipping steeper toward the surface where it correlates with the mapped fault trace (Barchi et al., 2021). The detachment zone in this area is again made up of two sub-horizontal shear faults that are vertically separated by about 1 km (black lines in Figure 4c; see also Figure 2d). The sequence of four M_W ~5.4 events (C1-4 in Figure 1a), all occurring within a 4-h time period, starts about 1.5 km above the detachment zone on the Campotosto segment of the Mt. Gorzano fault, a segment that was also active during the 2009 L'Aquila sequence (Valoroso et al., 2013). The events deepen with time of occurrence, with the second event, 50 min later, locating just below the first event, and the third event, 11 min later, just above the upper detachment fault. All three events exhibit low-angle normal faulting consistent with the lower Mt. Gorzano fault segment. The fourth Campotosto event occurred 3 h after the third event on or near the lower detachment fault with a dip slip focal mechanism. It lies on the same plane defined by the three previous events, suggesting that this latest event in the sequence images the structural complexities that arise from intersecting normal and detachment faults (Figure 4d). The timing of the events suggests that slip on the detachment fault occurs in response to slip on the normal faults, and thus the detachment zone can be considered as a passive structure, at least at this location of the fault system.

The piece-wise planar structure of the Mt. Gorzano fault, made up of kinked, planar segments a few km long (Figure 4c, cross sections 15 and 16 in Figure S1), is consistent with aftershock locations of the 2009 L'Aquila earthquake that triggered slip on the Campotosto fault segment (Valoroso et al., 2013). During that sequence, some of the larger events (M_W > 5) nucleated near the kinks, suggesting geometrical control on stress concentrations, and showed rotation of the P-axis with depth (Chiaraluce, 2012), confirming that the 2016–2017 sequence reactivated the piecewise planar, convex Mt. Gorzano fault. A similar fault geometry has been proposed for the Gualdo Tadino fault north of the 1997 Colfiorito system (Ciaccio et al., 2005), which, to our knowledge, is the only other example of an active, pseudo-listric normal fault imaged by seismicity. These observations support the hypothesis that large (M_W > 6) normal faulting earthquakes that rupture to the surface in the Apennines occur on near-planar faults, while structurally complex normal faults, like the Mt. Gorzano fault, are often blind and rupture in multiple, moderate size earthquakes (Buttinelli et al., 2021; Chiaraluce, 2012).

Detachments are commonly defined as extensional ramps cutting down sections in the direction of transport, showing no roots and usually following a stratigraphic horizon (Twiss & Moores, 1992). However, the prominent sub-horizontal structure that we refer to as detachment in this study does not strictly adhere to that definition. We see a sub-horizontal shear zone with no clear connection to the surface. The shear zone constitutes of sub-horizontal, fragmented faults that in some places are vertically offset and sometimes overlapping, suggesting a detachment emplaced along a lithological discontinuity that reactivates a previously compressive structure in the present-day extensional stress regime. The tectonic inversion of these large faults may be at the origin of a complex structural setting of the faults north of the ST and responsible for the main events of the 2016–2017 sequence. Faults show lower levels of correlated events (Figure 1c) and wider damage zones (0.91–1.74 km; Figure 3b) compared to the L'Aquila fault to the south (as narrow as 0.5 km; Valoroso et al., 2014), which is emplaced in a tectonically simpler setting. The heterogenous stress field generated by the complex tectonic history and the current fault mechanical interaction between inherited thrust structures, normal faults, and detachment therefore likely controls the complex faulting pattern along this part of the Apennine mountain belt.

Data Availability Statement

Earthquake catalog and fault planes presented are available at the Zenodo data set repository (https://doi.org/10.5281/zenodo.5091137). The waveform data from the Italian permanent and temporary stations are available through the European Integrated Data Archive (EIDA) at http://eida.ingv.it/it (station selection via interactive map for region shown in Figure 1a). Data from temporary stations deployed by the British Geological Survey (https://doi.org/10.7914/SN/YR_2016) are available from the Incorporated Research Institutions for Seismology Data Management System (http://ds.iris.edu).

References

Barchi, M. R., Alvarez, W., & Shimabukuro, D. H. (2012). The Umbria-Marche Apennines as a double orogen: Observations and hypotheses. *Italialian Journal of Geosciences (Boll. Soc. Geol. It.)*, *131*, 258–271. https://doi.org/10.3301/ijg.2012.17

Barchi, M. R., Carboni, F., Michele, M., Ercoli, M., Giorgetti, C., Porreca, M., et al. (2021). The influence of subsurface geology on the distribution of earthquakes during the 2016--2017 Central Italy seismic sequence. *Tectonophysics*, *807*, 228797. https://doi.org/10.1016/j.tecto.2021.228797

Berg, S. S., & Skar, T. (2005). Controls on damage zone asymmetry of a normal fault zone: Outcrop analyses of a segment of the Moab fault, SE Utah. *Journal of Structural Geology*, *27*, 1803–1822. https://doi.org/10.1016/j.jsg.2005.04.012

Buttinelli, M., Petracchini, L., Maesano, F. E., D'Ambrogi, C., Scrocca, D., Marino, M., et al. (2021). The impact of structural complexity, fault segmentation, and reactivation on seismotectonics: Constraints from the upper crust of the 2016–2017 Central Italy seismic sequence area. *Tectonophysics*, *810*, 228861. https://doi.org/10.1016/j.tecto.2021.228861

Calamita, F., Pace, P., & Satolli, S. (2012). Coexistence of fault-propagation and fault-bend folding in curve-shaped foreland fold-and-thrust belts: Examples from the northern Apennines (Italy). *Terra Nova*, *24*(5), 396–406. https://doi.org/10.1111/j.1365-3121.2012.01079.x

Carannante, S., Monachesi, G., Cattaneo, M., Amato, A., & Chiarabba, C. (2013). Deep structure and tectonics of the northern-central Apennines as seen by regional-scale tomography and 3-D located earthquakes. *Journal of Geophysical Research: Solid Earth*, *118*, 5391–5403. https://doi.org/10.1002/jgrb.50371

Cavinato, G. P., & DeCelles, G. (1999). Extensional basins in the tectonically bimodal central Apennines fold- thrust belt, Italy: Response to corner flow above a subducting slab in retrograde motion. *Geology*, *27*, 955–958. https://doi.org/10.1130/0091-7613(1999)027<0955:ebittb>2.3.co;2

Centamore, E., & Rossi, D. (2009). Neogene-quaternary tectonics and sedimentation in the central Apennines. *Bollettino della Societa Geologica Italiana*, *128*(1), 73–88. https://doi.org/10.3301/ijg.2009.128.1.73

Chiarabba, C., De Gori, P., Cattaneo, M., Spallarossa, D., & Segou, M. (2018). Faults geometry and the role of fluids in the 2016–2017 Central Italy seismic sequence. *Geophysical Research Letters*, *45*(14), 6963–6971. https://doi.org/10.1029/2018gl077485

Chiaraluce, L. (2012). Unravelling the complexity of Apenninic extensional fault systems: A review of the 2009 L'Aquila earthquake (Central Apennines, Italy). *Journal of Structural Geology*, *42*, 2–18. https://doi.org/10.1016/j.jsg.2012.06.007

Chiaraluce, L., Di Stefano, R., Tinti, E., Scognamiglio, L., Michele, M., Casarotti, E., et al. (2017). The 2016 Central Italy seismic sequence: A first look at the mainshocks, aftershocks, and source models. *Seismological Research Letters*, *88*(3), 757–771. https://doi.org/10.1785/022016022110.1785/0220160221

Chiaraluce, L., Ellsworth, W. L., Chiarabba, C., & Cocco, M. (2003). Imaging the complexity of an active normal fault system: The 1997 Colfiorito (Central Italy) case study. *Journal of Geophysical Research*, *108*(B6), 2294. https://doi.org/10.1029/2002JB002166

Ciaccio, M. G., Barchi, M. R., Chiarabba, C., Mirabella, F., & Stucchi, E. (2005). Seismological, geological and geophysical constraints for the Gualdo Tadino fault, Umbria–Marche apennines (central Italy), *Tectonophysics*, *406*(3–4), 233–247. https://doi.org/10.1016/j.tecto.2005.05.027

Cooper, C., & Burbi, L. (1986). Geology of the central Sibillini Mountains. *Memorie della Società Geologica Italiana*, *35*, 323–347.

Cosentino, D., Asti, R., Nocentini, M., Gliozzi, E., Kotsakis, T., Mattei, M., et al. (2017). New insights into the onset and subsequent evolution of the central Apennine extensional intermontane basins from the tectonically active L'Aquila Basin (central Italy). *Geological Society of America Bulletin*, *129*, 1314–1336. https://doi.org/10.1130/B31679.1

De Luca, G., Cattaneo, M., Monachesi, G., & Amato, A. (2009). Seismicity in the Umbria-Marche region from the integration of national and regional seismic networks. *Tectonophysics*, *476*(1), 219–231. https://doi.org/10.1016/j.tecto.2008.11.032

Ghisetti, F., & Vezzani, L. (1991). Thrust belt development in the Central Apennines: Northward polarity of thrusting and out-of-sequence deformations in the Gran Sasso chain (Italy). *Tectonics*, *10*, 904–919. https://doi.org/10.1029/91tc00902

Improta, L., Latorre, D., Margheriti, L., Nardi, A., Marchetti, A., et al. (2019). Multi-segment rupture of the 2016 Amatrice-Visso-Norcia seismic sequence (central Italy) constrained by the first high-quality catalog of Early Aftershocks. *Science*, *9*, 6921. https://doi.org/10.1038/s41598-019-43393-2

ISIDe Working Group. (2007). *Italian Seismological Instrumental and Parametric Database (ISIDe). Istituto Nazionale di Geofisica e Vulcanologia (INGV)*. https://doi.org/10.13127/ISIDE

Koopman, A. (1983). Detachment tectonics in the central Apennines. *Italy Geologica Ultraiectina*, *30*, 1–155.

Lavecchia, G. (1985). Il sovrascorrimento dei Monti Sibillini: Analisi cinematica e strutturale. *Bollettino della Società Geologica Italiana*, *104*, 161–194.

Lavecchia, G., Boncio, P., Brozzetti, F., Stucchi, M., & Leschiutta, I. (2002). New criteria for seismotectonic zoning in Central Italy: Insights from the Umbria-Marche Apennines. *Bollettino Società Geologica Italiana*, *1*, 881–890. Spec. Pub.

Lavecchia, G., Brozzetti, F., Barchi, M., Keller, J., & Menichetti, M. (1994). Seismotectonic zoning in east-central Italy deduced from the analysis of the Neogene to present deformations and related stress fields. *The Geological Society of America Bulletin*, *106*, 1107–1120. https://doi.org/10.1130/0016-7606(1994)106<1107:szieci>2.3.co;2

Lomax, A., Virieux, J., Volant, P., & Berge, C. (2000). Probabilistic earthquake location in 3D and layered models: Introduction of a Metropolis-Gibbs method and comparison with linear locations. In C. H. Thurber, & N. Rabinowitz (Eds.), *Advances in seismic event location* (pp. 101–134). Kluwer. https://doi.org/10.1007/978-94-015-9536-0_5

Malagnini, L. & Munafò, I. (2018). On the relationship between M_L and M_w in a broad range: An example from the Apennines, Italy. *Bulletin of the Seismological Society of America, 108* (2): 1018–1024. https://doi.org/10.1785/0120170303

Mazzoli, S., Pierantoni, P., Borraccini, F., Paltrinieri, W., & Deiana, G. (2005). Geometry, segmentation pattern and displacement variations along a major Apennine thrust zone, central Italy. *Journal of Structural Geology*, *27*, 1940–1953. https://doi.org/10.1016/j.jsg.2005.06.002

Mendoza, C., & Hartzell, S. H. (1988). Aftershock pattern and mainshock faulting. *Bulletin of the Seismological Society of America*, *78*, 1438–1449. https://doi.org/10.1785/bssa0780031092

Michele, M., Chiaraluce, L., Di Stefano, R., & Waldhauser, F. (2020). Fine-scale structure of the 2016–2017 Central Italy seismic sequence from data recorded at the Italian National Network. *Journal of Geophysical Research: Solid Earth*, *125*, e2019JB018440. https://doi.org/10.1029/2019JB018440

Michele, M., Di Stefano, R., Chiaraluce, L., Cattaneo, M., De Gori, P., Monachesi, G., et al. (2016). The Amatrice 2016 seismic sequence: A preliminary look at the mainshock and aftershocks distribution. *Annals of Geophysics*, *59*. https://doi.org/10.4401/ag-7227

Mildon, Z. K., Roberts, G. P., Faure Walker, J. P., & Iezzi, F. (2017). Coulomb stress transfer and fault interaction over millennia on non-planar active normal faults: The M_w 6.5–5.0 seismic sequence of 2016–2017, central Italy. *Geophysical Journal International*, *210*, 1206–1218. https://doi.org/10.1093/gji/ggx213

Moretti, M., Baptie, B., & Segou, M. (2016). SISMIKO: Emergency network deployment and data sharing for the 2016 central Italy seismic sequence. *Annales de Geophysique*, *59*(5). https://doi.org/10.4401/ag-7212

Page, M. T., Dunham, E. M., & Carlson, J. M. (2005). Distinguishing barriers and asperities in near-source ground motion. *Journal of Geophysical Research*, *110*, B11302. https://doi.org/10.1029/2005JB003736

Pino, N. A., Convertito, V., & Madariaga, R. (2019). Clock advance and magnitude limitation through fault interaction: The case of the 2016 central Italy earthquake sequence. *Scientific Reports*, *9*, 5005. https://doi.org/10.1038/s41598-019-41453-1

Porreca, M., Fabbrizzi, A., Azzaro, S., Pucci, S., Del Rio, L., Pierantoni, P. P., et al. (2020). 3D geological reconstruction of the M. Vettore seismogenic fault system (Central Apennines, Italy): Cross-cutting relationship with the M. Sibillini thrust. *Journal of Structural Geology*, *131*, 103938. ISSN 0191-8141. https://doi.org/10.1016/j.jsg.2019.103938

Pucci, S., De Martini, P. M., Civico, R., Villani, F., Nappi, R., Ricci, T., et al. (2017). Coseismic ruptures of the 24 August 2016, MW 6.0 Amatrice earthquake (Central Italy). *Geophysical Research Letters*, *44*, 2138–2147. https://doi.org/10.1002/2016gl071859

Sánchez-Reyes, H., Essing, D., Beaucé, E., & Poli, P. (2021). The imbricated foreshock and aftershock activities of the Balsorano (Italy) M_w 4.4 normal fault earthquake and implications for earthquake initiation. *Seismological Research Letters*, *92*, 1926–1936. https://doi.org/10.1785/0220200253

Schaff, D. P., & Waldhauser, F. (2005). Waveform cross-correlation-based differential travel-time measurements at the Northern California seismic network. *Bulletin of the Seismological Society of America*, *95*, 2446–2461. https://doi.org/10.1785/0120040221

Scognamiglio, L., Tinti, E., Casarotti, E., Pucci, S., Villani, F., Cocco, M., et al. (2018). Complex fault geometry and rupture dynamics of the M_w 6.5, 30 October 2016, Central Italy earthquake. *Journal of Geophysical Research: Solid Earth*, *123*(4), 2943–2964. https://doi.org/10.1002/2018jb015603

Scognamiglio, L., Tinti, E., & Michelini, A. (2009). Real-time determination of seismic moment tensor for the Italian region. *Bulletin of the Seismological Society of America*, *99*(4), 2223–2242. https://doi.org/10.1785/0120080104

Spallarossa, D., Cattaneo, M., Scafidi, D., Michele, M., Chiaraluce, L., Segou, M., & Main, I. G. (2020). An automatically generated high-resolution earthquake catalogue for the 2016-2017 Central Italy seismic sequence, including P and S phase arrival times. *Geophysical Journal International*, *225*, 555–571. https://doi.org/10.1093/gji/ggaa604

Supino, M., Festa, G., & Zollo, A. (2019). A probabilistic method for the estimation of earthquake source parameters from spectral inversion: Application to the 2016–2017 Central Italy seismic sequence. *Geophysical Journal International*, *218*(2), 988–1007. https://doi.org/10.1093/gji/ggz206

Tan, Y. J., Waldhauser, F., Ellsworth, W. L., Zhang, M., Zhu, W., Michele, M., et al. (2021). Machine-learning-based high-resolution earthquake catalog reveals how complex fault structures were activated during the 2016–2017 Central Italy sequence. *The Seismic Record*, *1*(1), 11–19. https://doi.org/10.1785/0320210001

Tinti, E., Scognamiglio, L., Michelini, A., & Cocco, M. (2016). Slip heterogeneity and directivity of the ML 6.0, 2016, Amatrice earthquake estimated with rapid finite-fault inversion. *Geophysical Research Letters*, *43*, 10745–10752. https://doi.org/10.1002/2016GL071263

Totaro, C., Seeber, L., Waldhauser, F., Steckler, M., Gervasi, A., Guerra, I., et al. (2015). An intense earthquake swarm in the Southernmost Apennines: Fault architecture from high-resolution hypocenters and focal mechanisms. *Bulletin of the Seismological Society of America*, *105/6*, 3121–3128. https://doi.org/10.1785/0120150074

Twiss, R. J., & Moores, E. M. (1992). *Structural geology* (p. 532). W.H. Freeman & Company.

Valoroso, L., Chiaraluce, L., & Collettini, C. (2014). Earthquakes and fault zone structure. *Geology*, *42*(4), 343–346. https://doi.org/10.1130/G35071.1

Valoroso, L., Chiaraluce, L., Piccinini, D., Di Stefano, R., Schaff, D., & Waldhauser, F. (2013). Radiography of a normal fault system by 64,000 high-precision earthquake locations: The 2009 L'Aquila (Central Italy) case study. *Journal of Geophysical Research: Solid Earth*, *118*, 1156–1176. https://doi.org/10.1002/jgrb.50130

Villani, F., Civico, R., Pucci, S., Pizzimenti, L., Nappi, R., De Martini, P. M., & De Martini, P. M. (2018). A database of the coseismic effects following the 30 October 2016 Norcia earthquake in Central Italy. *Scientific data*, *5*(1), 180049. https://doi.org/10.1038/sdata.2018.49

Vuan, A., Sugan, M., Chiaraluce, L., & Di Stefano, R. (2017). Loading rate variations along a midcrustal shear zone preceding the Mw6.0 earthquake of 24 August 2016 in Central Italy. *Geophysical Research Letters*, *44*, 12170–12180. https://doi.org/10.1002/2017GL076223

Waldhauser, F. (2001). HypoDD: A program to compute double-difference hypocenter locations. *U.S. Geological Survey Open-File Report*, 01–113.

Waldhauser, F., & Ellsworth, W. L. (2000). A double-difference earthquake location algorithm: Method and application to the northern Hayward Fault, California. *Bulletin of the Seismological Society of America*, *90*, 1353–1368. https://doi.org/10.1785/0120000006

Waldhauser, F., & Schaff, D. P. (2008). Large-scale relocation of two decades of Northern California seismicity using cross-correlation and double-difference methods. *Journal of Geophysical Research*, *113*, B08311. https://doi.org/10.1029/2007JB005479

Waldhauser, F., Wilcock, W. S. D., Tolstoy, M., Baillard, C., Tan, Y. J., & Schaff, D. P. (2020). Precision seismic monitoring and analysis at axial seamount using a real-time double-difference system. *Journal of Geophysical Research*, *124*, e2019JB018796. https://doi.org/10.1029/2019JB018796

Walters, R. J., Gregory, L. C., Wedmore, L. N. J., Craig, T. J., McCaffrey, K., Wilkinson, M., et al. (2018). Dual control of fault intersections on stop-start rupture in the 2016 Central Italy seismic sequence. *Earth and Planetary Science Letters*, *500*, 1–14. https://doi.org/10.1016/j.epsl.2018.07.043

Wernicke, B., & Burchfiel, B. C. (1982). Modes of extensional tectonics. *Journal of Geodynamics*, *4*(2), 105–115. https://doi.org/10.1016/0191-8141(82)90021-9